

Benzimidazole Derivatives in Identifying Novel Acetylcholinesterase Inhibitors: A Combination of 3D-QSAR, Docking and Molecular Dynamics Simulation

K. El Khatabi^a, R. El-Mernissi^a, I. Aanouz^a, M.A. Ajana^{a,*}, T. Lakhli^a, M. Shahinozzaman^b and M. Bouachrine^{a,c}

^a*Molecular chemistry and Natural Substances Laboratory, Faculty of Science, University Moulay Ismail, Meknes, Morocco*

^b*Department of Nutrition and Food Science, University of Maryland, College Park, MD 20742, USA*

^c*EST Khenifra, Sultan Moulay Sliman University, Beni Mellal, Morocco*

(Received 14 March 2021, Accepted 5 November 2021)

Acetylcholinesterase is a promising therapeutic candidate for the treatment of neurodegenerative disorders, acetylcholine dysfunction, and other cognitive problems. In the current study, a 3D-QSAR approach was applied to a series of benzimidazole derivatives to reveal the key influencing factors contributing to their acetylcholinesterase inhibition activity and selectivity. The developed two models, CoMFA and CoMSIA, were found to be internally validated using a training set of compounds, and both models demonstrated significant statistical reliability. Contour maps of developed models were employed to examine the main structural characteristics of inhibitors that affected their potency. It was found that electrostatic and hydrophobic interactions are significantly important for improving the inhibitory activities, leading to the design of four novel acetylcholinesterase inhibitors. Among the newly designed compounds, compound A1 with the highest predicted activity was subjected to detailed molecular docking and compared to the most active compound. Furthermore, 100 ns molecular dynamics (MD) simulation was conducted to explore the binding modes and conformational modifications throughout the interaction of compound A1 and acetylcholinesterase. The docking and MD simulation findings showed that the newly designed compound A1 remained stable within the active site of the identified acetylcholinesterase receptor, demonstrating its promising role as a new potential acetylcholinesterase drug candidate.

Keywords: Molecular modeling, Computational chemistry, Alzheimer's disease, Acetylcholinesterase, Benzimidazole

INTRODUCTION

Alzheimer's disease (AD) is a chronic persistent neurodegenerative disorder, which is a highly complicated dementia affecting millions of people worldwide with an increasing tendency [1]. AD, the most prevalent type of dementia among the elderly, is a progressive neurodegenerative disorder of the central nervous system caused by a degenerative brain condition [2]. AD typically presents as a progressive decline of memory initially, which is followed or accompanied by cognitive impairments,

executive problems, mood disturbances, impaired linguistic efficacy, visuospatial abnormalities, and other cognitive dysfunctions which eventually lead to death [3-5]. Although the pathogenesis of AD is still unknown, researchers have discovered that several factors are believed to play a crucial role in its initiation and progression. Low acetylcholine (ACh) levels, neurofibrillary tangles caused by tau-hyper phosphorylation as well as amyloid- β (A β) deposits and its extracellular plaques, oxidative stress, and amyloid β protein aggregation are considered as the characteristic pathological manifestations [6-9]. Acetylcholine is an essential neurotransmitter highly correlated with memory function and learning process [10]. At the cellular level, cholinergic deficiency in the synaptic process is associated

*Corresponding author. E-mail: a.ajanamohammed@fs.umi.ac.ma

with AD, reducing cortical cholinergic neurotransmission [11]. Improvement of the activity of cholinergic neurons seems to be the only way to develop potent drugs for the management of AD. It is carried out by modulating the levels of the neurotransmitter acetylcholinesterase (AChE) in the central nervous system. Acetylcholinesterase is a crucial enzyme that rapidly breaks down the neurotransmitter acetylcholine and ultimately terminates the cholinergic transmission on the postsynaptic membrane [12]. Inhibition of AChE causes acetylcholine accumulation in the synapses; this enhances the effects of acetylcholine, enhances the cholinergic nervous system function, and induces intellectual capabilities [13]. Thus, inhibition of AChE represents an important target for the control of AD.

To date, several AChE inhibitors have been reported, among which, *o/p*-propoxyphenylsubstituted-1H-benzimidazole derivatives developed by Sarikaya *et al.* [14] have been paid much more attention as AChE inhibitors to evaluate the cholinesterase inhibition activity. A series of 45 benzimidazole derivatives with potent and selective affinity for acetylcholinesterase has been selected for this study to derive a relationship between their structures and activities in detail. Several computational approaches have been applied through DFT and 3D-QSAR for optimizing and finding novel molecules as potent acetylcholinesterase inhibitors. The detailed binding modes of benzimidazole compounds against acetylcholinesterase were explored to ensure the reliability of the 3D-QSAR analysis through molecular docking and MD simulation. This study is expected to provide theoretical guidance for the exploration, prediction, and design of novel agonists against acetylcholinesterase.

MATERIALS AND METHODS

Experimental Data

A dataset of 45 benzimidazole derivatives previously evaluated for acetylcholinesterase inhibition activity IC₅₀ (μM) was selected for this study [14]. The 36 compounds were utilized as the training set for model generation, and the remaining 9 compounds were utilized as an independent test set (superscript * in Table 1) or for model validation. The experimental AChE inhibition activity was converted into pIC₅₀, so as to be used as a dependent variable in the QSAR analysis. The structures and experimental activity

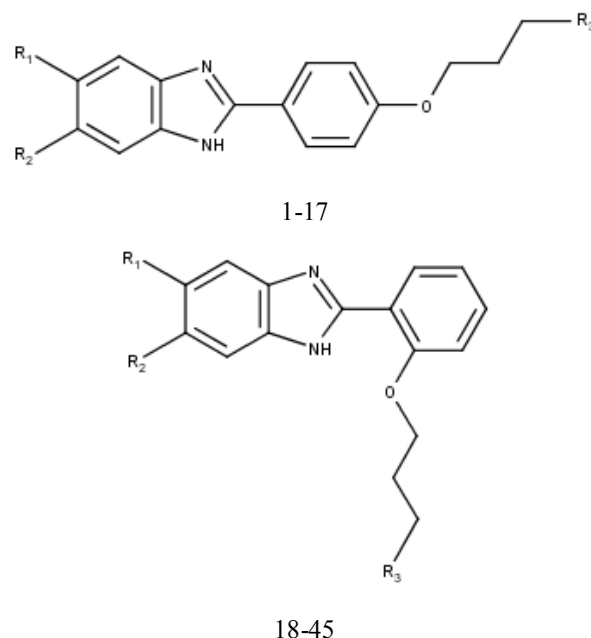


Fig. 1. Chemical structures of the studied compounds.

values of compounds are listed in Table 1. Figure 1 shows the chemical structures of the studied compounds.

Minimization and Optimization

The structures were built using the SYBYL-X 2.0 program and optimized under Tripos force field by energy minimization [15,16]. The convergence criterion assigned to these structures by Gasteiger-Huckel was 0.01 kcal mol⁻¹ [17]. The most active and designed compounds, employed as a data set for the following studies, were optimized by the DFT method B3LYP/6.311(d,p) basis set level using Gaussian software (09, Gaussian Inc., Wallingford, CT, USA) to achieve the equilibrium geometry for each compound [18].

Molecular Alignment

3D structural alignment is one of the most important steps used to derive robust and reliable 3D-QSAR models. Herein, compound 11 with the strongest AChE inhibitory activity was utilized as the structural template and its 2-phenylbenzimidazole analogue was set as a common core for alignment using the simple alignment method in Sybyl [19]. The minimized structures were employed for CoMFA and CoMSIA analyses as the primal conformations.

Table 1. Chemical Structures of Benzimidazole Derivatives with (AChE) Inhibitory Activities

No.	Position	R ₁	R ₂	R ₃	pIC ₅₀
1*	<i>Para</i>	H	H	-N(C ₂ H ₅) ₂	5.12
2	<i>Para</i>	H	H	Pyrrolidine	5.12
3	<i>Para</i>	H	H	Piperidine	5.07
4	<i>Para</i>	CH ₃	H	-N(C ₂ H ₅) ₂	5.55
5	<i>Para</i>	CH ₃	H	Pyrrolidine	5.19
6	<i>Para</i>	CH ₃	H	Piperidine	5.35
7	<i>Para</i>	Cl	H	Pyrrolidine	5.57
8	<i>Para</i>	Cl	H	Piperidine	5.58
9	<i>Para</i>	NO ₂	H	-N(C ₂ H ₅) ₂	6.53
10	<i>Para</i>	NO ₂	H	Pyrrolidine	6.52
11	<i>Para</i>	NO ₂	H	Piperidine	6.85
12*	<i>Para</i>	CN	H	-N(C ₂ H ₅) ₂	6.29
13	<i>Para</i>	CN	H	Pyrrolidine	6.02
14	<i>Para</i>	CN	H	Piperidine	6.16
15	<i>Para</i>	OCH ₃	OCH ₃	-N(C ₂ H ₅) ₂	6.05
16	<i>Para</i>	OCH ₃	OCH ₃	Pyrrolidine	6.35
17	<i>Para</i>	OCH ₃	OCH ₃	Piperidine	5.75
18*	<i>Ortho</i>	H	H	-N(CH ₃) ₂	5.13
19*	<i>Ortho</i>	H	H	-N(C ₂ H ₅) ₂	5.18
20	<i>Ortho</i>	H	H	Pyrrolidine	4.14
21	<i>Ortho</i>	H	H	Piperidine	5.09
22	<i>Ortho</i>	H	H	Morpholine	4.95
23*	<i>Ortho</i>	CH ₃	H	-N(CH ₃) ₂	5.15
24*	<i>Ortho</i>	CH ₃	H	-N(C ₂ H ₅) ₂	5.11
25*	<i>Ortho</i>	CH ₃	H	Pyrrolidine	5.14
26	<i>Ortho</i>	CH ₃	H	Piperidine	5.23
27	<i>Ortho</i>	CH ₃	H	Morpholine	4.08
28	<i>Ortho</i>	Cl	H	-N(CH ₃) ₂	5.13
29	<i>Ortho</i>	Cl	H	-N(C ₂ H ₅) ₂	5.18
30	<i>Ortho</i>	Cl	H	Pyrrolidine	4.19
31	<i>Ortho</i>	Cl	H	Piperidine	5.2
32	<i>Ortho</i>	NO ₂	H	-N(CH ₃) ₂	4.98
33	<i>Ortho</i>	NO ₂	H	-N(C ₂ H ₅) ₂	5.12
34	<i>Ortho</i>	NO ₂	H	Pyrrolidine	5.54
35	<i>Ortho</i>	NO ₂	H	Piperidine	4.92
36*	<i>Ortho</i>	NO ₂	H	Morpholine	4.71
37	<i>Ortho</i>	CN	H	-N(CH ₃) ₂	5.12
38	<i>Ortho</i>	CN	H	-N(C ₂ H ₅) ₂	5.13
39	<i>Ortho</i>	CN	H	Piperidine	4.25
40	<i>Ortho</i>	CN	H	Morpholine	5.12
41	<i>Ortho</i>	OCH ₃	OCH ₃	-N(CH ₃) ₂	4.18
42	<i>Ortho</i>	OCH ₃	OCH ₃	-N(C ₂ H ₅) ₂	5.11
43*	<i>Ortho</i>	OCH ₃	OCH ₃	Pyrrolidine	4.13
44	<i>Ortho</i>	OCH ₃	OCH ₃	Piperidine	5.05
45	<i>Ortho</i>	OCH ₃	OCH ₃	Morpholine	5.09

*Test molecules.

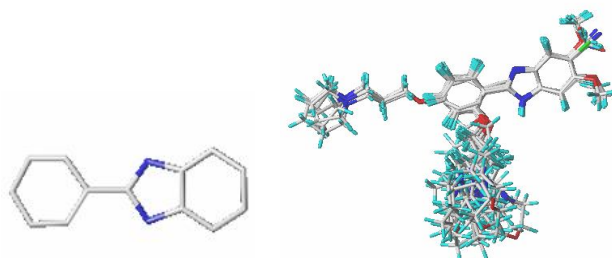
**Fig. 2.** Core (left) and aligned molecules (right) using molecule 11 as a structural template.

Figure 2 shows the core and superimposed structures of aligned molecules.

Development of 3D-QSAR Models

In the present work, the 3D-QSAR study was carried out using the two most classical methods in SYBYL, CoMFA, and CoMSIA upon the alignments to correlate the structures with inhibitory activity [20,21]. CoMSIA and CoMFA analysis were developed to analyze quantitatively the steric, electrostatic, hydrogen bond acceptor (HBA) hydrogen bond donor (HBD), and hydrophobic effects fields. 3D-QSAR analysis was performed using SYBYL in standard settings. As a final point, partial least square analysis was performed in which the value of column filtering was set at 2.0 kcal mol⁻¹ with 30 kcal mol⁻¹ as the y cutoff [22].

Partial Least Square (PLS) Analysis

PLS analysis method was adopted to build a linear relationship between the structural parameters and biological activities [23]. The optimum number of components (N) and the coefficient of cross-validation correlation (Q²) were calculated by the leave-one-out (LOO) method. The correlation coefficient (R²), the standard error of estimate (SEE) and the F-test value (F) were obtained by the non-cross validation procedure using the previously acquired N value. Hence, the optimal resulting 3D-QSAR model was chosen on the basis of the high values of Q² and R² (Q² > 0.50 and R² > 0.60) [24,25]. Additionally, an optimal number of components and low standard error estimation (SEE) are required conditions for a robust QSAR model with more reliable predictability. External validation was also employed to assess the reliability of the generated models by the testing set, as it is the most valuable validation process, where the required condition (r_{ext}² > 0.6)

must be satisfied [26].

Y-Randomization Test

The Y-Randomization test is generally utilized to confirm the strength of the generated models [27]. The dependent variable ($-\log IC_{50}$) is shuffled at random. The QSAR calculation process is replicated several times, yielding a new set of 3D-QSAR models for each iteration. The low values of Q^2 and R^2 indicate the efficiency and reliability of the optimal models.

Molecular Docking

Molecular docking, as a powerful approach, was employed using the Surflex-Dock module/Sybyl 2.0 to discover the structural interaction mechanism between ligands and the AchE receptor. The optimized selected compounds obtained from the DFT study were the starting structures of each following simulation. The crystal structure of 1EVE was provided by the RSCB Protein Data Bank. Using the Discovery Studio 2016 software, all water molecules and the original ligand were separated from the protein, and the binding modes were visualized using PyMOL software [28,29]. The preparation steps for the docking protocol were applied to establish molecular docking. The AutoDock Vina method [30] was utilized to further validate the findings of surflex-dock docking analysis of selected ligands. The output from the studies of ligand-protein interactions was analyzed using the AutoDock Tools version 1.5.4 [31]. The binding conformation between the receptor and the newly designed molecule with the highest-dock score was studied and chosen for further MD simulation.

Molecular Dynamics (MD) Simulation

MD simulation was performed to analyze the stability and probe the dynamic conformational changes of the selected complexes using YASARA Dynamics software [32]. The protein-designed molecule complex obtained from

molecular docking was the initial structure used for MD simulation. The molecular receptor topology files were created using the Leap module. The force field parameters for MD simulation and data analysis were obtained using the AMBER 14 force field [33]. The simulation was run using a periodic boundary condition, with the cell size being 20 Å larger than the protein. During the MD simulations, the electrostatic interaction within the periodic boundary conditions was calculated using the particle-mesh Ewald (PME) method [34]. The system was solvated in a rectangular water box with TIP3P water molecules and neutralized by adding the appropriate counter ions (Cl^- or Na^+) at 298 K temperature. The TIP3P solvent system is known to afford the best experimental results with a combination of AMBER14 force field. Subsequently, the temperature was kept constant during the following production stages by using the Berendsen algorithm. Using the steepest gradient approach (5000 cycles), the minimization of the solvent system was carried out by the simulated annealing method to avoid possible crashes between heavy atoms. The cut-off radius and time step values were set at 0.8 Å and 1.25 fs for the overall simulations. Finally, each system was subjected to a 100 ns MD simulation, with the trajectory of the simulated system changing every 100 ps. The root-mean-square deviation (RMSD), root-mean-square fluctuation (RMSF), gyration radius (Rg), solvent accessible surface area (SASA), dihedral angle, and secondary structure analysis were recorded at 100 ns.

RESULTS AND DISCUSSION

3D-QSAR Analysis

Internal and external validations were important criteria for measuring the robustness of the 3D-QSAR model. The statistical results of the 3D-QSAR PLS analyses are presented in Table 2. The experimental and predicted pIC_{50} of molecules are listed in Table 3. Table 3 shows the

Table 2. PLS Statistics Parameters

Model	Q^2	R^2	SEE	F	N	r_{ext}^2	Fractions				
							Ster	Elect	Acc	Don	Hyd
CoMFA	0.655	0.870	0.283	73.759	1	0.731	0.564	0.436	-	-	-
CoMSIA	0.643	0.852	0.301	63.543	1	0.710	0.185	0.337	0.248	0.087	0.143

Table 3. Experimental and Predicted Activities of 45 Benzimidazole Analogues

No.	pIC50	CoMFA		CoMSIA	
		Predicted	Residuals	Predicted	Residuals
1*	5.12	5.21	-0.09	5.25	-0.13
2	5.12	5.41	-0.29	5.33	-0.21
3	5.07	4.90	0.17	4.90	0.17
4	5.55	5.69	-0.14	5.68	-0.13
5	5.19	5.49	-0.3	5.48	-0.29
6	5.35	5.46	-0.11	5.48	-0.13
7	5.57	5.62	-0.05	5.61	-0.04
8	5.58	6.02	-0.44	5.97	-0.39
9	6.53	6.29	0.24	6.32	0.21
10	6.52	6.32	0.20	6.38	0.14
11	6.85	6.36	0.49	6.39	0.44
12*	6.29	6.11	0.18	6.13	0.16
13	6.02	6.18	-0.16	6.23	-0.21
14	6.16	6.06	0.10	6.09	0.07
15	6.05	5.99	0.06	5.95	0.10
16	6.35	6.11	0.24	6.10	0.25
17	5.75	5.84	-0.09	5.77	-0.02
18*	5.13	4.72	0.41	4.81	0.32
19*	5.18	5.56	-0.38	5.53	-0.35
20	4.14	4.14	0	4.19	-0.05
21	5.09	4.99	0.10	4.93	0.16
22	4.95	4.65	0.30	4.75	0.20
23*	5.15	5.25	-0.10	5.18	-0.03
24*	5.11	5.18	-0.07	5.09	0.02
25*	5.14	5.20	-0.06	5.13	0.01
26	5.23	5.03	0.20	4.94	0.29
27	4.08	4.33	-0.25	4.29	-0.21
28	5.13	5.18	-0.05	5.12	0.01
29	5.18	5.38	-0.20	5.28	-0.10
30	4.19	4.35	-0.16	4.34	-0.15
31	5.20	5.40	-0.20	5.32	-0.12
32	4.98	5.16	-0.18	5.32	-0.34
33	5.12	5.05	0.07	5.12	0
34	5.54	5.37	0.17	5.37	0.17
35	4.92	5.24	-0.32	5.24	-0.32
36*	4.71	4.63	0.08	4.65	0.06
37	5.12	5.07	0.05	5.15	-0.03
38	5.13	5.17	-0.04	5.26	-0.13
39	4.25	4.20	0.05	4.20	0.05
40	5.12	5.09	0.03	5.21	-0.09
41	4.18	4.09	0.09	4.20	-0.02
42	5.11	5.25	-0.14	5.20	-0.09
43*	4.13	4.12	0.01	4.12	0.01
44	5.05	5.20	-0.15	5.24	-0.19
45	5.09	5.20	-0.11	5.25	-0.16

experimental and predicted pIC50 of training and test set molecules.

For internal validation, the CoMFA model shows an acceptable cross-validation correlation Q^2 value of 0.655 for the training set with an excellent R^2 of 0.870, the lowest SEE of 0.283, F-test of 73.759 and N of 1, indicating that this generated model is reliable. The both steric and electrostatic fields contributed to 56.4% and 43.6% of the total contribution, respectively, revealing that the steric field played a more significant role. The best CoMSIA model had a Q^2 of 0.643 and an optimized component of 1, as well as an excellent R^2 of 0.852, the lowest SEE of 0.301, and F-test value of 63.543, which was indicative of the good internal predictability of this model. The ratios of steric, electrostatic, HBA, HBD, and hydrophobic sites in the model were 18.5%, 33.7%, 24.8%, 8.7%, and 14.3%, respectively, revealing that electrostatic and hydrophobic fields had a greater impact on the model.

External validation revealed that CoMFA and CoMSIA had excellent predictive power, with r_{ext}^2 values of 0.731 and 0.710, respectively, indicating that the external predictability of both models rose up to the standard.

Contour Map Analysis

The contour maps of the 3D-QSAR models could visually explore significant structural features for the improvement of activity. The structural modification process in certain areas based on the useful information provided by the contour maps would rationally guide lead optimization. The structure of compound 11 was overlaid on the contours as a reference for the explanation.

CoMFA contour maps. Figure 3a shows the CoMFA steric contour map, with green (80% contribution) and yellow (20% contribution) colors indicating sterically favorable and unfavorable contours, respectively. Compound 11 had a broad green contour around R3, illustrating that raising the volume at R3 would be beneficial to activity. Compound 11 (pIC50 = 5.658), for example, presented a large substituent in R3 and had higher activity than compounds 9 (pIC50 = 4.59) and 10 (pIC50 = 5.143). A yellow contour appeared at R1, which expressed the need to decrease the volume of R1. Therefore, compound 12 possessing a less bulky substituent in this position increases the potency.

Figure 3b shows the CoMFA electrostatic contour map,

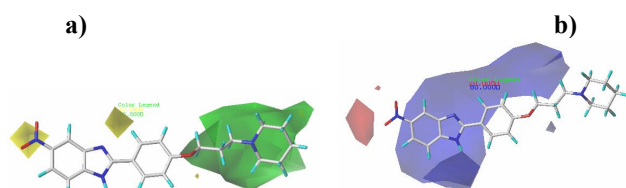


Fig. 3. Std*coeff. Contour maps of CoMFA analysis for compound 11. a) Steric fields; b) Electrostatic fields.

where the negative electrostatic favorable contours are represented in red (20% contribution) and the unfavorable contours in blue (80% contribution). There was a blue contour near the benzimidazole scaffold, indicating substituents with positive charges may improve the activity. This can be verified by the high value of activity of compound 16 holding the –OMe substituent over compound 7 (Cl), taking into consideration that both possess the same substituent (Pyrrolidine) at R3.

CoMSIA contour map. The steric and electrostatic contours of CoMFA provide similar findings to those of the CoMSIA model. As a result, only H-bonding and hydrophobic contour maps were investigated.

Figure 4a shows a hydrophobic contour map, with the white contours (20% contribution) indicating the favorable region for hydrophilic substituents and with the yellow contours (80% contribution) indicating an unfavorable region for hydrophilic substituents. There were two small white contours around R3, which indicated that the increase in the hydrophilicity of R3 could improve the activity. Furthermore, a yellow contour near the phenyl substitution in the *ortho* position of the benzimidazole scaffold indicated that increasing the hydrophobicity of the substituent would aid in the increase in activity in the corresponding regions.

H-bond acceptor and donor contour maps are shown in Fig. 4b and Fig. 4c, respectively. Cyan (80% contribution) and red (20% contribution) contours represent that adding H-bond donor groups has a positive effect on activity, while the purple (20% contribution) and magenta (80% contribution) contours denote that H-bond donor groups have a negative impact on potency. The purple contour around the nitro group (R1) showed that substituting an H-bond acceptor in this position could improve activity. The necessity of the H-bond donor –NH group was revealed by the red contour near the N position of benzimidazole, which

is beneficial to its inhibitory activity.

Y-Randomization Test

Table 4 shows the results of seven random shuffles for the Y-randomization test. The Q^2 and R^2 values obtained by the seven iterations were extremely low, according to the Y-randomization test. Consequently, the possibility of a chance correlation was ruled out, which indicates that the two obtained models are very trustworthy, good and highly reliable.

Newly Designed Compounds

The chemical information acquired from contour maps was utilized to define the structural features of acetylcholinesterase inhibitors to design new ligands with

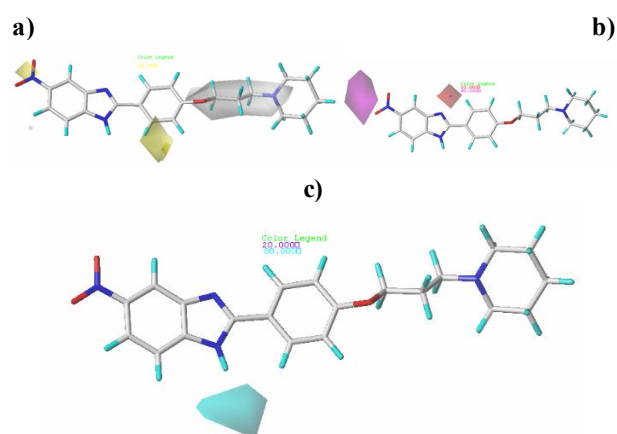


Fig. 4. Std*coeff. Contour maps of CoMSIA analysis for compound 11. a) Hydrophobic field; b) H-bond acceptor fields; c) H-bond donor fields.

Table 4. Q^2 and R^2 Values of the Y-Randomization Test

Iteration	CoMFA		CoMSIA	
	Q^2	R^2	Q^2	R^2
1	0.305	0.378	0.341	0.402
2	0.099	0.107	0.112	0.131
3	-0.088	0.102	-0.034	0.167
4	0.008	0.084	0.059	0.105
5	0.144	0.198	0.132	0.187
6	-0.105	0.125	-0.084	0.103
7	0.124	0.216	0.137	0.246

an increased potency profile. Hence, through modifying the R1, R2, and R3 structures of the benzimidazole scaffold, four new compounds with high acetylcholinesterase inhibitory activities have been designed in silico. Table 5 shows the structures of four newly designed inhibitors, their predicted activity, pIC₅₀, total score, as well as binding energy. The predicted activity values of the designed compounds were in the range of (6.912-6.859) and (6.870-6.827) for the CoMFA and CoMSIA models, respectively. The predicted activities of the four compounds were much greater not only than that of compound 11, but also than its experimental activity.

Molecular Docking

In the present study, to reveal the optimal binding patterns between small molecules and proteins, molecular docking was conducted using the Surflex-Dock method. The statistical result of molecular docking was expressed in Total Score, predicting the correlation of ligand-based on the structure of the receptor. As shown in Table 4, the newly designed compound A1 had a higher docking score than compound 11, which is in agreement with its predicted activity and AutoDock Vina score. The conformation that possessed the high Total Score (compound A1) was selected for further detailed analysis and compared to compound 11. Figure 5 depicts the active site of acetylcholinesterase,

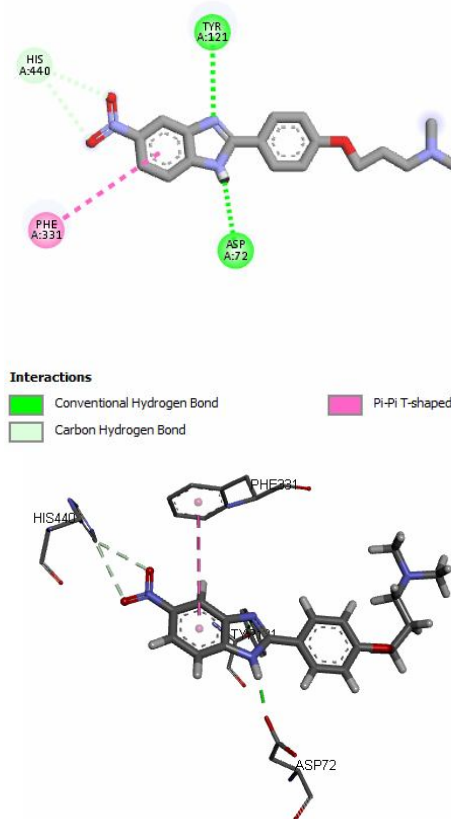


Fig. 5. 2D structure and interaction of designed compound A1 with acetylcholinesterase.

Table 5. New Proposed Molecules and their Predicted pIC₅₀, Total Score and Binding Energy

No.	R1	R2	R3	Predicted pIC ₅₀		Total score Surflex dock	Binding energy (kcal mol ⁻¹) Autodock Vina
				CoMFA	CoMSIA		
The most active compound							
Comp.11	NO ₂	H	Piperidine	6.36	6.39	4.6201	-7.3
The newly designed compounds							
A1	NO ₂	H	-N(CH ₃) ₂	6.912	6.870	4.7948	-7.4
A2	NO ₂	NH ₂	Piperidine	6.881	6.84	4.0395	-6.8
A3	CN	H	-N(CH ₃) ₂	6.862	6.827	4.2568	-7.3
A4	CN	NH ₂	-N(CH ₃) ₂	6.859	6.860	4.2903	-7.4

where the two nitrogen atoms of the piperidine ring in compound A1 form two hydrogen-bonding interactions with Tyr 121 and Asp 72. Obviously, these interactions are stabilizing interactions and beneficial for inhibitory activity. In addition, His 440 formed two carbon-hydrogen bonding interactions with the nitro group of the compound A1. Also, Phe 331 formed a π - π T-shaped interaction with the benzene moiety of the benzimidazole. The combination of these interactions significantly increases the stability of the binding. As depicted in Fig. 6, compound 11, as the most potent inhibitor in the series, showed a carbon-hydrogen bonding interaction with His 440. The $-O-$ linker connecting the piperidine ring and the right phenyl moiety formed a lone-pair- π bonding interaction with Phe 330. Another lone-pair- π bonding interaction made up by Phe 330 was in contact with the nitrogen atom of the phenyl moiety on the upper right side. In addition, the benzimidazole and central phenyl ring formed a π - π stacking effect with the residue Tyr 334. The binding of compound 11 has also been shown to be influenced by van der Waals and hydrophobic interactions. In comparison to compound 11, which has a stronger inhibitory effect on acetylcholinesterase, the newly designed compound A1 has more favorable and stabilizing interactions with the targeted protein. The docked poses of the newly designed compound A1 and compound 11 inside acetylcholinesterase were depicted in Fig. 5 and Fig. 6, respectively.

The docking findings were compared to the 3D-QSAR results to ensure that the two were in agreement. Thus, the binding interactions were consistent with hydrogen bonding and hydrophobic contour maps. These findings indicate that the newly designed compound A1 binds to the binding site of acetylcholinesterase with great compatibility. The docked conformation of the newly designed compound A1 with acetylcholinesterase was utilized as an input for molecular dynamics simulations.

Molecular Dynamics Simulation

To investigate the dynamic behavior of a protein after ligand binding, a 100 ns MD simulation was run using the protein-designed molecule complex A1 to ensure the stability of the predicted binding of the complex system. Figure 7a displays the RMSD of the heavy atoms of acetylcholinesterase over 100 ns. The RMSD of protein-

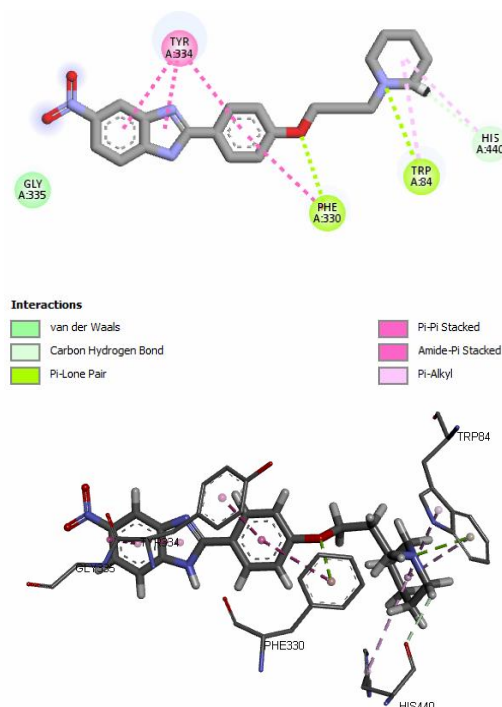


Fig. 6. 2D structure and interaction of compound 11 with acetylcholinesterase.

designed molecule complex A1 fluctuated between 0.42 and 1.68 Å during the MD simulations, and the averaged RMSD was found to be 1.43 Å. From 0 to 40 ns, the curve of complex A1 rose slightly to the value of approximately 1.68 Å, and then an equilibrated system was obtained in complex A1 within the rest of the time. RMSD analysis indicated that the designed molecule A1 formed a stable complex with the protein throughout the simulations.

To investigate the impact of designed molecule binding on the internal dynamics of the target protein during 100 ns, RMSF values were also calculated. It can be seen from Fig. 7b that a maximum fluctuation of 5.9 Å is noticed in the loop region of residue 550 and a high fluctuation of 4.6 Å is detected in the loop region close to residue 380. Although minimal fluctuations were observed during the interaction of protein and designed compound A1, most of these fluctuations were lower than 3 Å, indicating that the binding strength between compound A1 and protein is strong. Meanwhile, the protein was more affected by the movement of the corresponding ligand in the studied

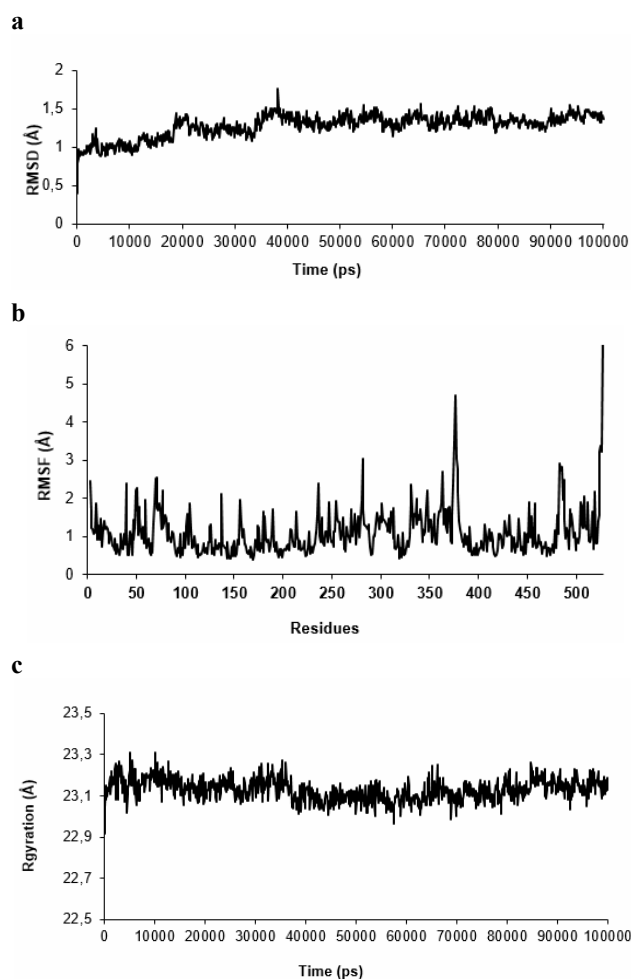


Fig. 7. MD simulation trajectory analysis. a. RMSD of the whole protein of protein-designed molecule complex. b. RMSF of protein-designed molecule complex. c. Rg of protein-designed molecule complex.

system. RMSF analysis indicated that binding of designed compound A1 to the target protein presented a slightly non-significant fluctuation, indicating that there were no significant changes in protein conformation as a result of the ligand binding.

The gyration radius (Rg), which represents the change in protein structure compactness over time, was measured (Fig. 7c). In the first 37 ns, the Rg values varied between 22.91 Å and 23.31 Å. However, after this time until the simulation ended, the values remained reasonably stable in

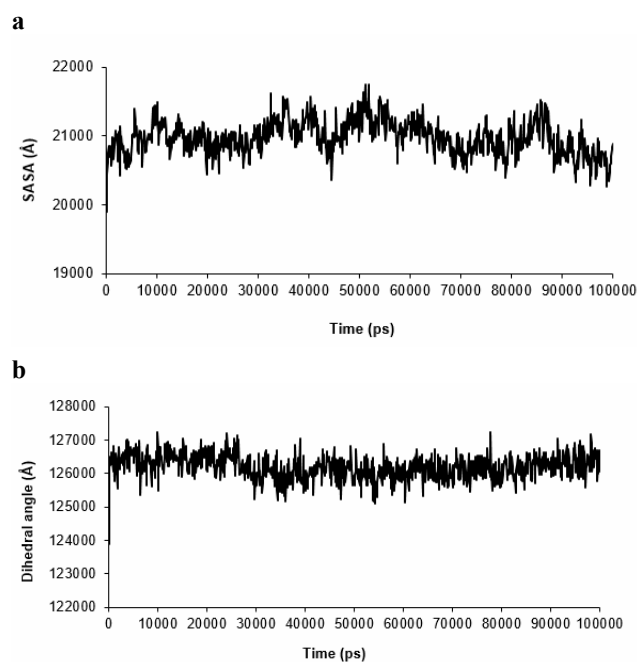


Fig. 8. Solvent accessible surface area (SASA) and dihedral angle. a. SASA of protein-designed molecule complex. b. Dihedral angle of protein-designed molecule complex.

the range of 22.96 to 23.26. The Rg graph shows that there is no major change in the compactness of the folding of the target protein after the binding of the designed molecule A1. Similarly, the SASA analysis was explored to identify the solvent accessibility of the protein-ligand complex (Fig. 8a). During the last 30 ns, SASA was observed to be in the range of 20486 to 213404 Å, with one fluctuation at 86 ns, and then stabilized as the simulation progressed, indicating the crucial role played by the major part of the newly designed compound A1 in the cavity of its binding to the receptor. This displays that the number of hydrophobic amino acids hidden inside the protein was basically unchanged and the structure of proteins was relatively stable after the binding of compound A1 to the catalytic pocket during the simulation time.

Furthermore, the dihedral angle of the protein-designed molecule was also studied to quantify the conformational flexibility of compound A1 when bound to acetylcholinesterase. As depicted in Fig. 8b, dihedral transitions were absent during the simulation and the

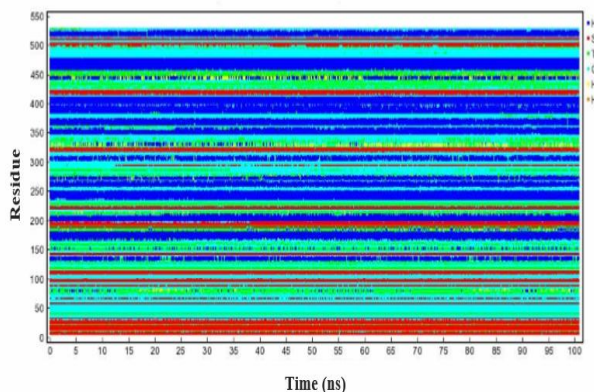


Fig. 9. Secondary structure analysis of protein-designed molecule complex.

average value of dihedral angle for compound A1 was found to be 126065. The results revealed that the system achieved equilibrium at about 29 ns and acetylcholinesterase in the studied system underwent very slight conformational changes as shown by the dihedral angle values. On the other hand, the evolution of dihedral angles of inhibitor in the system was more stable after 29 ns. This confirms that compound A1 is conformationally rigid.

Furthermore, we conducted secondary analysis of the studied complex to find out the changes in the secondary structures induced by the binding of the designed molecule (Fig. 9). In the study of the change in structural behavior, the percentage of secondary structure content in a protein is an essential metric. There was no significant change in the secondary structure content of the newly designed compound A1. However, binding of compound A1 to the acetylcholinesterase appears to result in a modest increase in the residue number in the structured region. The involvement of more amino residues at the binding site might be responsible for the stability of the ligand bound conformation of the targeted protein.

Comparison with Literature

For this class of acetylcholinesterase inhibitors, several researchers have designed and synthesized novel benzimidazole derivatives [35-39]. Through our SARs, molecular docking, and MD analyses, we have

demonstrated that the newly designed compounds reported in the present work exhibited higher acetylcholinesterase inhibitory activity than all of the synthesized benzimidazole derivatives in the literature. In addition, the newly designed compounds, in comparison with the previously synthesized benzimidazole derivatives, were more active and had more favorable and stabilizing interactions with the targeted protein.

Our study revealed the potential binding of the newly designed benzimidazole based-derivative at the active site of the target acetylcholinesterase protein. The newly designed compound A1 showed better interaction with the targeted protein, which was revealed by hydrogen bond formation, hydrophobic interaction, and docking pose of the compound A1. At the same time, active site residues in the binding site such as Tyr 121 and Asp 72 were involved in H-bond interactions with compound A1 and had a significant contribution to the binding process after R3 was modified. In addition, His 440 was involved in hydrophobic interactions with the same compound, which were found to play a crucial role in the firm binding of ligand to the receptor. Noticeably, the observed interactions are stabilizing interactions, which are beneficial for potency and could enable inhibitors to maintain stability in the binding site. Overall, the results of the current study indicate that compound A1 possesses acetylcholinesterase inhibition potential and could serve as a potential source of the lead molecules for anti-Alzheimer drug discovery. The detailed understanding of the complexity of ligand-receptor interactions might be attained by utilizing different ligand-binding assays such as structure-based (X-ray and NMR), label-free, labeled, and whole cell ligand-binding methods. So we firmly believe this is an important theoretical basis for designing novel benzimidazole derivatives as potent inhibitors of acetylcholinesterase for the treatment of Alzheimer disease.

CONCLUSIONS

In-silico analysis was used successfully to gain insight into the critical structural aspects of benzimidazole derivatives and their inhibition mechanism. The CoMFA and CoMSIA models developed in the 3D-QSAR study had satisfactory predictive ability. Based on the chemical

features unveiled by 3D-QSAR contour plot analysis, four novel inhibitors were designed by making appropriate substitutions for the benzimidazole derivative, among which compound A1 with the highest predicted activity was subjected to molecular docking, and their possible binding patterns were investigated and compared to those of the most active compound 11. Through prediction of activity and molecular docking, compound A1 was selected for detailed 100ns MD simulation analysis due to its highly predicted activity, docking score and binding affinity. The MD simulation analysis demonstrates that the ligand closely binds to the acetylcholinesterase active site, which confirms the stability of compound A1 within the biological environment throughout the MD simulation process. Consequently, the newly designed compound A1 was successfully identified as a potent acetylcholinesterase inhibitor.

ACKNOWLEDGEMENTS

We are grateful to the “Association Marocaine des Chimistes Théoriciens” (AMCT) for its pertinent help concerning the programs.

COMPETING INTERESTS

The authors declare that they have no competing interests.

REFERENCES

- [1] Sivakumar, M.; Saravanan, K.; Saravanan, V.; Sagarthi, S.; kumar, S. M.; Alhaji Isa, M.; Rajakumar, P.; Aravindhana, S., Discovery of new potential triplet acting inhibitor for alzheimer’s disease *via* X-ray crystallography, molecular docking and molecular dynamics, *J. Biomol. Struct. Dyn.*, **2020**, *38*, 1903-1917. DOI: 10.1080/07391102.2019.1620128.
- [2] Xu, Y.; Jian, M. -M.; Han, C.; Yang, K.; Bai, L.; Cao, F.; Ma, Z. -Y., Design, synthesis and evaluation of new 4-arylthiazole-2-amine derivatives as acetylcholinesterase inhibitors, *Bioorg. Med. Chem. Lett.*, **2020**, *30*, 126985. DOI: 10.1016/j.bmcl.2020.126985.
- [3] Huang, L. -K.; Chao, S. -P.; Hu, C. -J., Clinical trials of new drugs for alzheimer disease, *J. Biomed. Sci.*, **2020**, *27*, 18. DOI: 10.1186/s12929-019-0609-7.
- [4] Singh, A.; Sharma, S.; Arora, S.; Attri, S.; Kaur, P.; Kaur Gulati, H.; Bhagat, K.; Kumar, N.; Singh, H.; Vir Singh, J.; *et al.*, New coumarin-benzotriazole based hybrid molecules as inhibitors of acetylcholinesterase and amyloid aggregation, *Bioorg. Med. Chem. Lett.*, **2020**, *30*, 127477. DOI: 10.1016/j.bmcl.2020.127477.
- [5] Tramutola, A.; Lanzillotta, C.; Perluigi, M.; Butterfield, D. A., Oxidative stress, protein modification and alzheimer disease, *Brain Res. Bull.*, **2017**, *133*, 88-96. DOI: 10.1016/j.brainresbull.2016.06.005.
- [6] El Khatabi, K.; Aanouz, I.; El-mernissi, R.; Khaldan, A.; Ajana, M. A.; Bouachrine, M.; Lakhlifi, T., 3D-QSAR and molecular docking studies of *p*-aminobenzoic acid derivatives to explore the features requirements of alzheimer inhibitors, *Orbital Electron. J. Chem.*, **2020**, *12*, 172-181. DOI: 10.17807/orbital.v12i4.1467.
- [7] Choi, S. S.; Lee, S. -R.; Kim, S. U.; Lee, H. J., Alzheimer’s disease and stem cell therapy, *Exp. Neurobiol.*, **2014**, *23*, 45-52. DOI: 10.5607/en.2014.23.1.45.
- [8] Wang, Z.; Wang, Y.; Li, W.; Mao, F.; Sun, Y.; Huang, L.; Li, X., Design, synthesis, and evaluation of multitarget-directed selenium-containing clioquinol derivatives for the treatment of alzheimer’s disease, *ACS Chem. Neurosci.*, **2014**, *5*, 952-962. DOI: 10.1021/cn500119g.
- [9] Rosini, M.; Simoni, E.; Caporaso, R.; Minarini, A., Multitarget strategies in alzheimer’s disease: Benefits and challenges on the road to therapeutics, *Future Med. Chem.*, **2016**, *8*, 697-711. DOI: 10.4155/fmc-2016-0003.
- [10] Lotfi, S.; Rahmani, T.; Hatami, M.; Pouramiri, B.; Kermani, E. T.; Rezvannejad, E.; Mortazavi, M.; Fathi Hafshejani, S.; Askari, N.; Pourjamali, N.; *et al.*, Design, synthesis and biological assessment of acridine derivatives containing 1,3,4-thiadiazole moiety as novel selective acetylcholinesterase inhibitors, *Bioorganic Chem.*, **2020**, *105*, 104457. DOI: 10.1016/j.bioorg.2020.104457.
- [11] Sharma, K., Cholinesterase inhibitors as alzheimer’s

- therapeutics (Review), *Mol. Med. Rep.*, **2019**, *20*, 1479-1487. DOI: 10.3892/mmr.2019.10374.
- [12] Dvir, H.; Silman, I.; Harel, M.; Rosenberry, T. L.; Sussman, J. L., Acetylcholinesterase: From 3D structure to function, *Chem. Biol. Interact.*, **2010**, *187*, 10-22. DOI: 10.1016/j.cbi.2010.01.042.
- [13] Su, J.; Liu, H.; Guo, K.; Chen, L.; Yang, M.; Chen, Q., Research advances and detection methodologies for microbe-derived acetylcholinesterase inhibitors: A systemic review, *Molecules*, **2017**, *22*, 176. DOI: 10.3390/molecules22010176.
- [14] Sarıkaya, G.; Çoban, G.; Parlar, S.; Tarikogullari, A. H.; Armagan, G.; Erdoğan, M. A.; Alptüzün, V.; Alpan, A. S., Multifunctional cholinesterase inhibitors for Alzheimer's disease: Synthesis, biological evaluations, and docking studies of *o/p*-Propoxyphenylsubstituted-1H-Benzimidazole Derivatives, *Arch. Pharm. (Weinheim)*, **2018**, *351*, 1800076. DOI: 10.1002/ardp.201800076.
- [15] S TRIPOS Associates, Inc. 2012. Sybyl-X Molecular Modeling Software Packages., Version X-2.0. (accessed Feb 6, 2020).
- [16] Clark, M.; Cramer, R. D.; Van Opdenbosch, N., Validation of the general purpose tripos 5.2 force field, *J. Comput. Chem.*, **1989**, *10*, 982-1012. DOI: 10.1002/jcc.540100804.
- [17] Purcell, W. P.; Singer, J. A., A brief review and table of semiempirical parameters used in the hueckel molecular orbital method, *J. Chem. Eng. Data*, **1967**, *12*, 235-46. DOI: 10.1021/jc60033a020.
- [18] Lee, C.; Yang, W.; Parr, R. G., Development of the colle-salvetti correlation-energy formula into a functional of the electron density, *Phys. Rev. B*, **1988**, *37*, 785-789. DOI: 10.1103/PhysRevB.37.785.
- [19] AbdulHameed, M. D. M.; Hamza, A.; Liu, J.; Zhan, C.-G., Combined 3D-QSAR modeling and molecular docking study on indolinone derivatives as inhibitors of 3-phosphoinositide-dependent protein kinase-1, *J. Chem. Inf. Model.*, **2008**, *48*, 1760-1772. DOI: 10.1021/ci800147v.
- [20] Cramer, R. D.; Patterson, D. E.; Bunce, J. D., Comparative molecular field analysis (CoMFA). 1. Effect of shape on binding of steroids to carrier proteins, *J. Am. Chem. Soc.*, **1988**, *110*, 5959-5967. DOI: 10.1021/ja00226a005.
- [21] Klebe, G.; Abraham, U.; Mietzner, T., Molecular similarity indices in a comparative analysis (CoMSIA) of drug molecules to correlate and predict their biological activity, *J. Med. Chem.*, **1994**, *37*, 4130-4146. DOI: 10.1021/jm00050a010.
- [22] Stähle, L.; Wold, S., 6 Multivariate data analysis and experimental design in biomedical research, *Prog. Med. Chem., Elsevier*, **1988**, *25*, 291-338. DOI: 10.1016/S0079-6468(08)70281-9.
- [23] Bush, A. I., The metal theory of Alzheimer's disease, *J. Alzheimers Dis.*, **2012**, *33*, S277-S281. DOI: 10.3233/JAD-2012-129011.
- [24] Golbraikh, A.; Tropsha, A., Beware of Q²!, *J. Mol. Graph. Model.*, **2002**, *20*, 269-276. DOI: 10.1016/S1093-3263(01)00123-1.
- [25] Tropsha, A.; Gramatica, P.; Gombar, V., The importance of being earnest: Validation is the absolute essential for successful application and interpretation of QSPR models, *QSAR Comb. Sci.*, **2003**, *22*, 69-77. DOI: 10.1002/qsar.200390007.
- [26] Baroni, M.; Clementi, S.; Cruciani, G.; Costantino, G.; Riganelli, D.; Oberrauch, E., Predictive ability of regression models. Part II: Selection of the best predictive PLS model, *J. Chemom.*, **1992**, *6*, 347-356. DOI: 10.1002/cem.1180060605.
- [27] Rücker, C.; Rücker, G.; Meringer, M., Y-Randomization and its variants in QSPR/QSAR, *J. Chem. Inf. Model.*, **2007**, *47*, 2345-2357. DOI: 10.1021/ci700157b.
- [28] Dassault Systèmes BIOVIA, Discovery Studio Modeling Environment, Release 2017. San Diego: Dassault Systèmes, **2016**.
- [29] DeLano W. L., Pymol: An open-source molecular graphics tool. *CCP4 Newsletter Pro Crystallogr.*, **2002**, *40*, 82-92.
- [30] Trott, O.; Olson, A. J., AutoDock Vina: Improving the speed and accuracy of docking with a new scoring function, efficient optimization, and multithreading, *J. Comput. Chem.*, **2009**, *31*, 455-461. DOI: 10.1002/jcc.21334.
- [31] Morris, G. M.; Goodsell, D. S.; Halliday, R. S.; Huey, R.; Hart, W. E.; Belew, R. K.; Olson, A. J., Automated docking using a Lamarckian genetic algorithm and an

- empirical binding free energy function, *J. Comput. Chem.*, **1998**, *19*, 1639-1662. DOI: 10.1002/(SICI)1096-987X(19981115)19:14%3C1639::AID-JCC10%3E3.0.CO;2-B.
- [32] Krieger, E.; Darden, T.; Nabuurs, S. B.; Finkelstein, A.; Vriend, G., Making optimal use of empirical energy functions: Force-field parameterization in crystal space, proteins struct. *Funct. Bioinforma.*, **2004**, *57*, 678-683. DOI: 10.1002/prot.20251.
- [33] Case, D. A.; Cheatham, T. E.; Darden, T.; Gohlke, H.; Luo, R.; Merz, K. M.; Onufriev, A.; Simmerling, C.; Wang, B.; Woods, R. J., The amber biomolecular simulation programs, *J. Comput. Chem.*, **2005**, *26*, 1668-1688. DOI: 10.1002/jcc.20290.
- [34] Nam, K.; Gao, J.; York, D. M., An efficient linear-scaling ewald method for long-range electrostatic interactions in combined QM/MM calculations, *J. Chem. Theory Comput.*, **2005**, *1*, 2-13. DOI: 10.1021/ct049941i.
- [35] Alpan, A. S.; Parlar, S.; Carlino, L.; Tarikogullari, A. H.; Alptüzün, V.; Güneş, H. S., Synthesis, biological activity and molecular modeling studies on 1H-benzimidazole derivatives as acetylcholinesterase inhibitors. *Bioorg. Med. Chem.*, **2013**, *21*, 4928-4937. DOI: 10.1016/j.bmc.2013.06.065.
- [36] Sarıkaya, G.; Çoban, G.; Parlar, S.; Tarikogullari, A. H.; Armagan, G.; Erdoğan, M. A.; Alptüzün, V.; Alpan, A. S., Multifunctional cholinesterase inhibitors for alzheimer's disease: Synthesis, biological evaluations, and docking studies of *o/p*-propoxyphenylsubstituted-1H-benzimidazole derivatives. *Arch. Pharm. (Weinheim)*, **2018**, *351*, 1800076. DOI: 10.1002/ardp.201800076.
- [37] Adalat, B.; Rahim, F.; Taha, M.; Alshamrani, F. J.; Anouar, E. H.; Uddin, N.; Shah, S. A. A.; Ali, Z.; Zakaria, Z. A., Synthesis of benzimidazole-based analogs as anti alzheimer's disease compounds and their molecular docking studies. *Molecules*, **2020**, *25*, 4828. DOI: 10.3390/molecules25204828.
- [38] Acar Cevik, U.; Sağlık, B.; Levent, S.; Osmaniye, D.; Kaya Cavuşoğlu, B.; Ozkay, Y.; Kaplancikli, Z., Synthesis and AChE-inhibitory activity of new benzimidazole derivatives. *Molecules*, **2019**, *24*, 861. DOI: 10.3390/molecules24050861.
- [39] Yoon, Y. K.; Ali, M. A.; Wei, A. C.; Choon, T. S.; Khaw, K. -Y.; Murugaiyah, V.; Osman, H.; Masand, V. H., Synthesis, characterization, and molecular docking analysis of novel benzimidazole derivatives as cholinesterase inhibitors. *Bioorganic Chem.*, **2013**, *49*, 33-39. DOI: 10.1016/j.bioorg.2013.06.008.